

Ultra-Broad Schmidt Modes for Biphoton States Generated by SPDC in the Chirped QPM Crystals

Jinbao Wang^{1,2}, Zhan Zheng^{2*}, Helin Wang^{2**}, Qiang Lin^{2***}

1. College of Mechanical Engineering, Zhejiang University of Technology, Hangzhou 310023, China

2. Zhejiang Province Key Laboratory of Quantum Precision Measurement, College of Physics, Zhejiang University of Technology, Hangzhou 310023, China

* zhan@zjut.edu.cn

** whlin@zjut.edu.cn

***qlin@zjut.edu.cn

Abstract

In the realm of quantum optics, the manipulation and characterization of biphoton states hold significant importance for advancing quantum information processing and communication technologies. This study explores the Schmidt decomposition of ultra-broad biphoton states, revealing that most modes are fulfilled with the frequency response points, and certain modes exhibit exceptionally broad Schmidt spectra. These Schmidt modes in frequency domain are significantly reshaped and widened by a crystal at a moderate chirp-rate when pump bandwidth is about several Giga-Hertz.

Keywords: biphoton, SPDC, Schmidt modes

1. Introduction

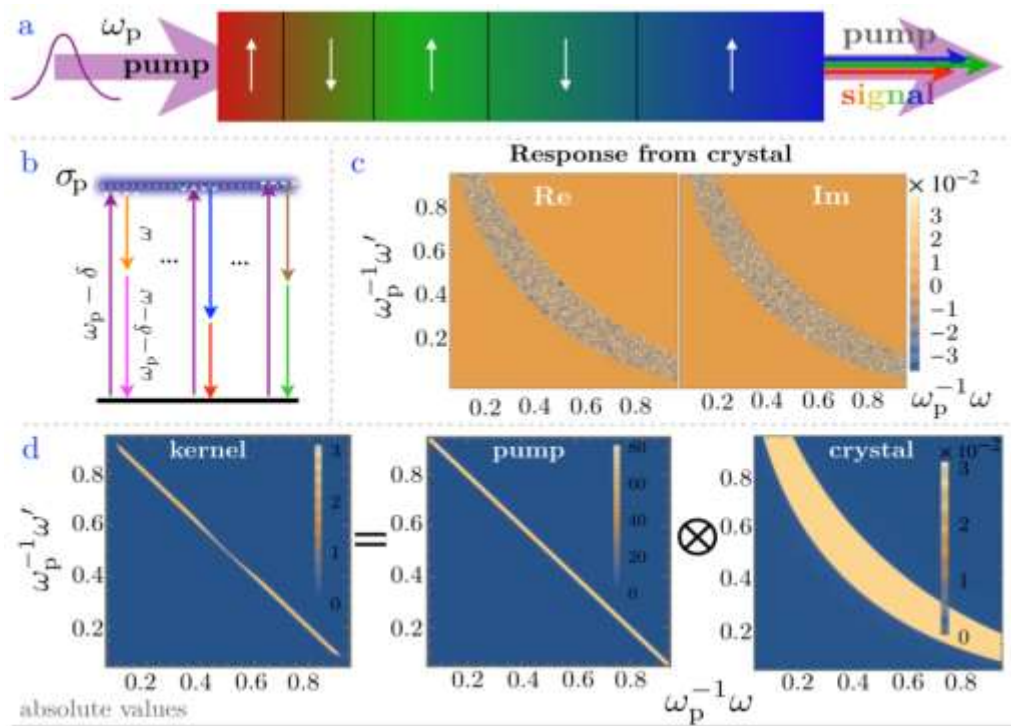
Multimode states are vital resources in quantum optics[1]. Broadband frequency modes/short temporal modes are ideal candidates to take advantage of the multimodality of optical states. To date, ultrashort quantum pulses of few cycle[2-4], single cycle[5-7], and even subcycle[8] levels are successfully generated. Though with some developments in classical theory[9], fundamental tests[10-11], and ultrafast applications[12-14], subcycle regime of quantum nonlinear optics is still challenging, due to the lack of subcycle sources.

Biphoton states[15], generated by spontaneous parametric down-conversion(SPDC), have the characteristic of nonclassical physics and have been widely studied and applied in theory and experiment. In particular, there is a strong correlation between the signal and idler photons generated in the SPDC process, as well as a high degree of entanglement in space and frequency[16-17]. It makes them be attractive and widely applied in quantum optics, quantum information and quantum measurement[18-19]. The broadband of spectrum for the biphoton, reaches the terahertz (THz) in

32 frequency, shows many non-classical physical properties and opens up entirely new perspectives[20-
 33 22]. In order to better control and modulate the spatial and spectral characteristics of the biphoton, the
 34 method for quantifying the entanglement based on the Schmidt decomposition has been shown in
 35 Ref.[23-24]. The eigenvectors have been reduced single particle density matrices which are named as
 36 Schmidt modes. The pure single particle Schmidt mode can be formed with a complete orthogonal
 37 basis, and each one can be related with an exact counterpart[25]. Broadband biphoton states are
 38 widely generated with short pump pulses in SPDC process[26]. The spectra can be broadened by
 39 using chirping quasi-phase matching(QPM) crystals[27], and even with (quasi-) monochromatic
 40 pump, the biphoton pulses can be generated at the single cycle level[28-29] in many Schmidt modes.

41 2. Theory

42 To investigate the physical characteristics of biphoton generated by SPDC in the chirped QPM
 43 periodically poled lithium niobate (PPLN) crystal, we set a Gaussian pulse with bandwidth ω_p as a
 44 pump beam passing through the chirped QPM PPLN crystal, analysis how does the various pump
 45 bandwidths and chirped rate influence with the physical characteristics of biphoton in multi-mode
 46 during the SPDC process.



47
 48 Figure.1 (a).Gaussian pump propagating through the chirped QPM PPLN crystal and splitting into signal and idler pulses during
 49 SPDC; (b). Schematic diagram of the down conversion for the pump, signal and idler pulses; (c). the real and imaginary parts for the
 50 response function of chirped QPM PPLN crystal; (d). the kernel of the biphoton state amplitude(BSA) function can be viewed as the
 51 product of pump function and phase matching function of the crystal.

52 As shown in Fig.1(a): in a SPDC process inside a linearly chirped QPM PPLN crystal of length L ,
53 the poled gratings varying along the propagating z axis, with the alternately opposite poled directions.
54 A photon of a generic frequency ω'_p from a classical strong pump field(central frequency ω_p ,
55 bandwidth σ_p) can split in two: a photon of frequency ω and a partner of frequency $\omega'_p - \omega$, and
56 vice versa. The spatial frequency of the crystal is $K_0 + \zeta z$, where ζ is the chirping parameter,
57 similar to the cases in Ref.[6,28,30]. And K_0 is the initial value, which is the poled period in the
58 entrance face of the crystal, matches with the incident pulse frequency $\frac{2\pi}{\Lambda_c}$ to make phase
59 compensation[28]. Following the procedures[26,29,31], the biphoton state reads

$$60 \quad |bi\rangle = T_0 \iint d\omega dw T(\omega, w) \hat{a}^\dagger(\omega) \hat{a}^\dagger(w) |0\rangle \quad (1)$$

61 Here, \hat{a}^\dagger is the creation operator of frequency ω , and T_0 the normalization coefficient. **Similar to**
62 **the assumption in Ref.[28], the pump light can be treated as quasi-monochromatic, the frequency of**
63 **the pump light can be approximately equal to the sum of the frequencies of the signal and the idler**
64 **lights.** As the Gaussian can be viewed as quasi-monochromatic laser if the bandwidth σ_p is rather
65 narrower compared with the central frequency ω_p of pump light. And the relations between the
66 frequencies for these three pulses associated with σ_p is shown in Fig.1(b). With the conditions of the
67 collinear propagation of the three pulses without consideration for Poynting vector walk-off, we can
68 set this case with noncritical type II QPM configuration[17] and the creation operator \hat{a}^\dagger , which
69 operated by the interaction between the pulses with the chirped QPM PPLN, is slowly varying with
70 the distance, and the phase matching function $\Phi(\omega, w)$ can be expressed as follows[28]

$$71 \quad \Phi(\omega, w) = \int_0^L \exp\left(\frac{i\zeta z^2}{2} + i\Delta kz\right) dz \quad (2)$$

72 where $\Delta k = k(\omega + w) - k(\omega) - k(w) - K_0$ is the phase mismatching involves the phases of
73 the three mixed waves and could be matched with the poled period of the crystal. $k(\omega)$ is the wave-
74 numbers of lights at frequency ω , which is determined by the refractive indices from the Sellmeier
75 equations by $k(\omega) = n\omega/c$.

76 The biphoton state amplitude(BSA) function $T(\omega, w) = \alpha(\omega, w) \Phi(\omega, w)$ has two parts: the

77 spectral envelope $\alpha(\omega, w) = \sqrt{\frac{1}{\pi\sigma^2}} \exp\left[-\frac{(\omega + w - \omega_p)^2}{2\sigma^2}\right]$, and the phase-matching kernel[6]

$$78 \quad \Phi(\omega, w) = \frac{\exp\left(\frac{\Delta k(\omega, w)^2}{2i\zeta}\right)}{\sqrt{2\zeta}} \left\{ \operatorname{erfi}\left[\frac{\zeta L + \Delta k(\omega, w)}{\sqrt{-2i\zeta}}\right] - \operatorname{erfi}\left[\frac{\Delta k(\omega, w)}{\sqrt{-2i\zeta}}\right] \right\} \quad (3)$$

79 When the chirping parameter ζ is negligibly small, the nonlinear optical processes take place
80 efficiently as some specific frequencies satisfying the conditions $\omega + w = \omega_p$ as well as

81 $\Delta k(\omega, w) = 0$, then the phase-matching kernel becomes sinc functions, which is well-known in the

82 Ref.[32]. However, in general cases, the phase matching kernel can be dramatically different due to

83 the chirping parameter: the phase-matching kernel is a highly oscillation function for both frequency

84 arguments ω and w in a wide region, giving birth to many fine ripples. Even near the line

85 $\omega + w = \omega_p$, the function $\Phi(\omega, \omega_p - \omega)$ is still highly oscillating, see Fig.1(c). As ζz is the

86 compensation of spatial frequency by the crystal, any mismatch $\Delta k(\omega, w)$ from $-\zeta L$ to 0 can

87 fulfill the phase-matching condition $\Delta k(\omega, w) + \zeta z = 0$ at a certain position. As a result, the

88 SPDC processes take place in the active zone $-\zeta L \leq \Delta k(\omega, w) \leq 0$, which can also be known

89 from the properties of Fresnel integral. With larger chirping parameter ζ , more frequencies are

90 allowed to be down-converted from the pump. **It allows the phase mismatching with wider frequency**

91 **range to be compensated, which further expands the frequency response range of the biphoton.** One

92 then concludes that the frequencies contribute to the SPDC processes quite equally in the presence of

93 chirp.

94 The BSA is a function with complicated quadratic phase mismatching factor caused by the

95 interaction between the chirped QPM PPLN crystal and the three waves' phase mismatching. And the

96 chirped QPM plays a substantial roles for this special part. There would be an inevitable ultrabroad

97 response frequency caused by the chirped poled periods for the QPM PPLN crystal.

98 The BSA function $T(\omega, w)$ can be operated by Schmidt decomposition with the product of the
 99 orthogonal eigen basis in the form of ω and w . $T(\omega, w)$ can be expressed by the eigen basis of T
 100 written as follows[31]

$$101 \quad T(\omega, w) = \sum_n \sqrt{\lambda_n} u_n(\omega) v_n(w) \quad (4)$$

102 Where λ_n is the eigenvalue corresponding the Schmidt modes u_n and v_n which defined as the
 103 eigenvectors for the signal and idler photons.

104 Schmidt decomposition is expected to quantize calculate the entanglement[17,31,33,34] generated
 105 by SPDC. This decomposition process for SPDC involves two factors: the bandwidth of pump pulse
 106 and the structure of the nonlinear crystal. For the bandwidth of pump, it means that the frequencies of
 107 signal and idler would be independent and not be one-one matching. However, they often show strong
 108 correlation for both of them are related to the frequency of pump pulse. The correlation range of
 109 frequency for idler light is restricted by the bandwidth of pump light, and the detected signal
 110 frequency[34].

111 The biphoton amplitude is symmetric, $T(\omega, w) = T(w, \omega)$, since $\Delta k(\omega, w) = \Delta k(w, \omega)$. It
 112 enables one to make the following Schmidt decomposition

$$113 \quad T_0 T(\omega, w) = \sum_{n=1}^{\infty} \sqrt{\frac{\lambda_n}{2}} u_n(\omega) u_n(w), \quad \lambda_1 \geq \lambda_2 \geq \dots \geq 0 \quad (5)$$

114 where $\sqrt{\lambda_n}, u_n(\omega)$ are known as the Schmidt coefficients and the Schmidt modes respectively,
 115 satisfying $\int u_m^*(\omega) u_n(\omega) d\omega = \delta_{mn}$. As a result, the biphoton state can be expressed as

$$116 \quad |bi\rangle = \sum_{n=1}^{\infty} \sqrt{\lambda_n} |2 : u_n\rangle \quad (6)$$

117 where $|n : u_k\rangle$ are distinguishable Fock states with n photons in the mode u_k , and the
 118 coefficients satisfy $\sum_{n=1}^{\infty} \lambda_n = 1$.

119 In literature, the Schmidt number $K = 1/\sum_n \lambda_n^2$ is known as a good measure of entanglement in
 120 pure biphoton states, and is can also be calculated in the following way

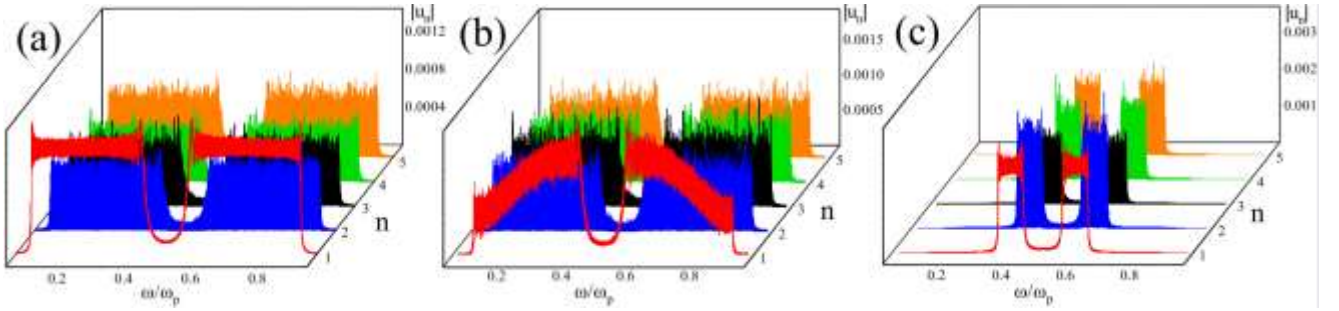
121
$$K = \frac{\left[\iint |T(\omega, w)|^2 d\omega dw \right]^2}{\iint \left| \int T(\omega, \omega') T^*(\omega', w) d\omega' \right|^2 d\omega dw}$$
 (7)

122 When the spectral bandwidth of the pump is much smaller than the typical distance between two
 123 neighboring ripples in the phase-matching kernel, the spectral envelope $\alpha(\omega, w)$ become a narrow
 124 peak function along the line $\omega + w = \omega_p$. Because $\alpha(\omega_p - \omega, \omega_p - w) = \alpha(\omega, w)$, the biphoton
 125 amplitude should satisfy

126
$$T(\omega, w) \approx T(\omega_p - \omega, \omega_p - w)$$
 (8)

127 One may then introduce an analogue of the parity operator $\hat{\beta}$ about the frequency center $\omega_p/2$:
 128 $\hat{\beta}f(\omega) = f(\omega_p - \omega)$ for any function f . Because $\hat{\beta}^2 = 1$, the parity operator $\hat{\beta}$ has two
 129 eigenvalues ± 1 . Consequently, the Schmidt coefficients should be degenerate, and the Schmidt
 130 modes can be of odd parity or even parity.

131 3. Results and Analysis

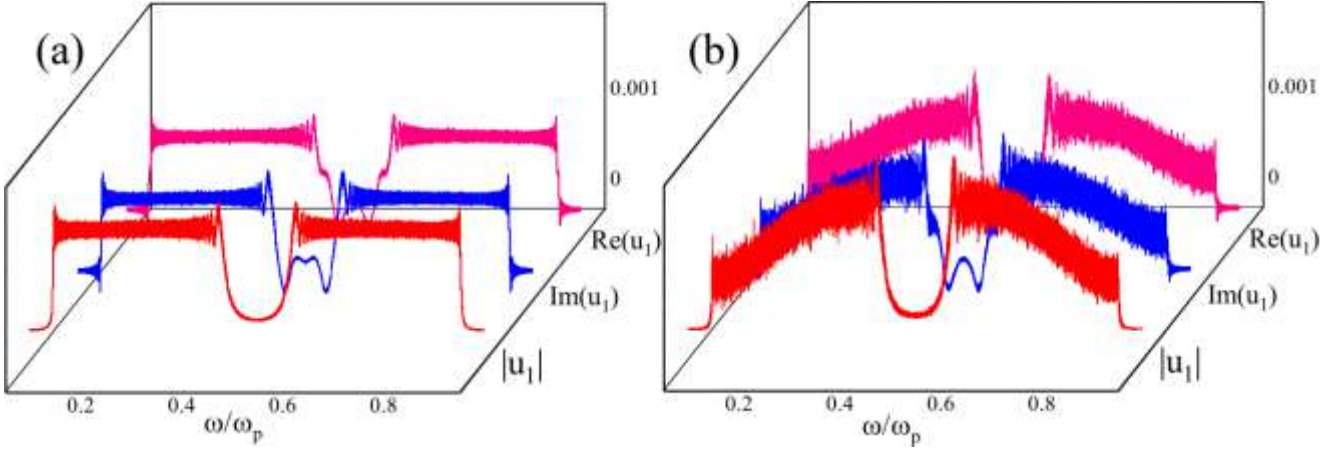


132
 133 Figure 2. The Schmidt modes distributions with (a). $\sigma_p = 2\pi\text{GHz}$ and $\zeta = 56\text{mm}^{-2}$;
 134 (b). $\sigma_p = 20\pi\text{GHz}$ and $\zeta = 56\text{mm}^{-2}$; (c). $\sigma_p = 2\pi\text{GHz}$ and $\zeta = 5.6\text{mm}^{-2}$.

135 Most modes show the FFRP structures of spectral distribution except $n = 1$.

136 The Schmidt decomposition of wavefunction for biphoton shows a remarkable property that the
 137 probability of the particles in Schmidt modes within corresponding condition in the range of
 138 $0 \rightarrow 100\%$ [33], it means that if the one of pairs photons can be detected in Schmidt mode u_n , and
 139 another photon can be detected, within the certain probability in adjoint mode v_n in the same mode
 140 index. And the biphoton probability is represented by the $\sqrt{\lambda_n}$ of Schmidt decomposition in the
 141 modes $\{u_n, v_n\}$ [33]. The entangled photons can be probed in the homologous modes with certain

142 probability as the entangled one has been detected in the same index. The entanglement can be
 143 detected between the two independent frequencies. In this paper, we only consider the pairs in the
 144 homologous modes for the two entangled biphoton, the vector value of λ_n represents the paired
 145 probability in the same modulus index[31]. Of course some other peculiar parameters such as
 146 azimuthal angles which shows orbital angular movement in SPDC configuration has been considered
 147 and discussed in Ref.[17], would be ignored in this paper.



148

149

Figure.3. The real and imaginary parts of the Schmidt modes $n = 1$ with the chirp rate $\zeta = 56\text{mm}^{-2}$

150

and the pump bandwidth is set as (a). $\sigma_p = 2\pi\text{GHz}$; (b). $\sigma_p = 20\pi\text{GHz}$.

151

152

153

Fig.2(a) to (c) shows the Schmidt modes distributions in various cases, one may notice that the Schmidt modes shown in these Figures are symmetrically distributed with the $\omega/\omega_p = 0.5$ and generated biphoton with ultrabroad bandwidth.

154

155

156

157

158

159

160

161

162

163

164

It can be found by the simulation that with the appropriate chirp rate, the spectral response frequency $\Delta\omega$ is relatively wide in each Schmidt mode of entangled biphoton generated by SPDC in chirped QPM crystal. The most common structures spectral distribution in Schmidt modes are filled with full frequency response points (FFRP) distribution. The FFRP distribution represents the response point corresponding to each frequency, but the response amplitude of each point is different, and the amplitude values oscillate between 0 and the maximum value. With some specific conditions, such as when the pumping bandwidth is GHz shown in this paper, the similar structure spectral distribution can be detected in some special Schmidt modes which has been described in Ref.[28,30].

From Fig.2, it can be found that the distribution of the first mode is clearer and more symmetrical, and its frequency response range $\Delta\omega$ is mainly depended on the chirp rate of the QPM crystal. The chirp rate increase can effectively expand the frequency response range $\Delta\omega$ for the reason of the

165 chirped poled grating periods can effectively compensate the phase mismatching of biphoton with
166 more frequency. By comparison, when the pumping optical bandwidth $\sigma_p = 2\pi GHz$ and $20\pi GHz$,
167 its impact on the frequency response range $\Delta\omega$ is not obvious, the main reason is that the center
168 frequency of the pumping optical reaches the THz level, the pumping bandwidth of GHz and 10GHz
169 is extremely narrow compared with THz, the difference is not particularly obvious, so the impact on
170 the frequency response $\Delta\omega$ is also relatively limited. However, the difference in pumping optical
171 bandwidth will cause the distribution of spectral power in different modes. The main reason is that the
172 bandwidth of the pump laser can affect the frequency relationship between the pump, signal and idler
173 lights. For example, the mode distribution of $n = 1$ in Fig.2 is a very obvious difference. It means
174 that the corresponding amplitudes are larger, with a higher response probability. In particular, when
175 the pumping optical bandwidth $\sigma_p = 2\pi GHz$, the pumping light is closer to the monochromatic
176 light than that at $\sigma_p = 20\pi GHz$. The spectral frequency distribution in this mode is also closer to the
177 biphoton spectral distribution obtained by SPDC with the monochromatic pump light as described in
178 Ref.[28,30]. The spectrum distribution in the first mode cannot be clearly defined if the pumping
179 bandwidth is too narrow or too wide, and the appropriate pumping bandwidth can be used as an
180 approximation of the monochromatic light, such as σ_p is GHz or 10GHz levels in the paper.
181 Through the two comparisons, it can be found that when the pumping bandwidth $\sigma_p = 20\pi GHz$, the
182 spectral amplitude of the left and right sides of the generated biphoton with a frequency of $\omega_p/2$ is
183 slightly higher, and the middle of the original double-rectangular distribution is improved.

184 With the increase of the modulus index n , the distribution of each mode shows less different,
185 and the frequency response range $\Delta\omega$ is almost consistent, and all of them fill the entire spectral
186 frequency space. By comparing different Schmidt modes with different pump bandwidths and
187 different chirp rates, it can be found that the main spectral form is FFRP distribution, and the spectral
188 distribution described in Ref. [28,30] can be obtained only in some specific modes with modulus
189 index $n = 1$ mode, and the other modes are basically FFRP distribution. The frequency response
190 range $\Delta\omega$ is consistent in different modes with the same chirp rate and pump bandwidth. Therefore,
191 a basic conclusion can be drawn that the chirp rate is the main factor affecting the frequency response
192 range in the SPDC of chirped QPM crystals when the pump light is determined.

193 Table.1 specifically describes the variation of the ratio of spectral response range $\Delta\omega$ to the
 194 center frequency of the pump light in different modes with different chirp rates and pumping
 195 bandwidth. By comparison, it can be found that the chirp rate of the QPM crystal is the main decisive
 196 factor. When the chirp rate is small, the frequency response range $\Delta\omega$ is also narrower, narrower
 197 than the center frequency of the pump light. As the chirp rate increases, the frequency response range
 198 $\Delta\omega$ becomes wider, even wider than the center frequency of the pump light. Meanwhile, the
 199 frequency response range $\Delta\omega$ with the same chirp rate and pump bandwidth in different modes are
 200 almost consistent. A slightly wider of the frequency response range $\Delta\omega$ could be slightly wider in
 201 modulus index $n = 1$, but not particularly obvious.

$\zeta (mm^{-2})$	5.6	56	
$\sigma_p (GHz)$	2π	2π	20π
Modulus Index	$\Delta\omega/\omega_p$		
$n = 1$	0.7191	1.2435	1.2416
$n = 2$	0.7189	1.2410	1.2370
$n = 3$	0.7182	1.2410	1.2370
$n = 4$	0.7172	1.2366	1.2385
$n = 5$	0.7160	1.2406	1.2401

202 Table.1. The frequency response bandwidth per central frequency of pump light signed as

203 $\Delta\omega/\omega_p$ in some Schmidt modes

204 In the bi-rectangular spectral distribution, the absolute value, the real part and the imaginary part
 205 also show similar distributions in this mode (see Fig.3). There are two main differences: First, at the
 206 central frequency $\omega_p/2$, both the real part and the imaginary part slightly oscillate, but for the
 207 absolute value, the oscillation part disappears, forming a bi-rectangular spectral distribution similar to
 208 that in Ref. [28,30]. Another difference is that at low frequency and high frequency, both the real and
 209 the imaginary parts have spectral distribution, but the distribution oscillates near 0. However, for the
 210 spectral distribution in absolute value, the value at low frequency and high frequency becomes 0
 211 again.

212 **4. Conclusion**

213 As the investigation of Schmidt mode distributions for biphoton generated by SPDC in the chirped
214 QPM crystals, theoretical results show that the pulses have rich structures in many modes. Most
215 distributions are fulfilled with the frequency response points. These Schmidt modes in frequency
216 domain are significantly reshaped and widened by the crystal at a moderate chirp-rate. These
217 broadband spectral distributions in Schmidt modes help us to obtain temporal ultrashort pulses with
218 few-, single- or even sub- cycles. The results provide some insights into this special optical process,
219 and can be helpful to quantum technologies.

220 **Conflicts of interests**

221 The authors declare no conflicts of interests.

222 **Acknowledgements**

223 This work was supported by the Joint Funds of the National Natural Science Foundation of China
224 under Grant U2341246. The first author would like to sincerely thank S. E. Harris for his Mathematica
225 codes.

226 **Funding**

227 This work was funded by the Joint Funds of the National Natural Science Foundation of China under
228 Grant U2341246.

229 **Data availability statement**

230 Necessary data are included in this article. Other data will be available from the corresponding authors
231 upon reasonable request.

232 **Authors' contributions**

233 Jinbao Wang simulated and calculated this work, and wrote the article. Zhan Zheng and Helin Wang
234 contributed to design and supervise this work. Qiang Lin participated in the discussions about this
235 work and reviewed the manuscript.

236 **References**

- 237 [1]. Fabre C, Treps N, Modes and states in quantum optics, *Rev. Mod. Phys.* 92, 035005 (2020).
238 <https://doi.org/10.1103/RevModPhys.92.035005>
- 239 [2]. Wenger J, Tualle-Brouri R, Grangier P, Pulsed homodyne measurements of femtosecond squeezed pulses generated
240 by single-pass parametric deamplification, *Opt. Lett.* 29, 1267–1269 (2004). <https://doi.org/10.1364/OL.29.001267>
- 241 [3]. Pinel O et al., Generation and characterization of multimode quantum frequency combs, *Phys. Rev. Lett.* 108, 083601
242 (2012). <https://doi.org/10.1103/PhysRevLett.108.083601>
- 243 [4]. Iskhakov T et al., Generation and direct detection of broadband mesoscopic polarization190 squeezed vacuum, *Phys.*
244 *Rev. Lett.* 102, 183602 (2009). <https://doi.org/10.1103/PhysRevLett.102.183602>
- 245 [5]. Shverdin MY et al., Generation of a single-cycle optical pulse, *Phys. Rev. Lett.* 94, 033904 (2005).
246 <https://doi.org/10.1103/PhysRevLett.94.033904>

- 247 [6]. Nasr MB et al., Ultrabroadband biphoton generated via chirped quasi-phase-matched optical parametric down-
248 conversion, *Phys. Rev. Lett.* 100, 183601 (2008). <https://doi.org/10.1103/PhysRevLett.100.183601>
- 249 [7]. Sensarn S, Yin GY, Harris SE, Generation and compression of chirped biphoton, *Phys. Rev. Lett.* 104, 253602 (2010).
250 <https://doi.org/10.1103/PhysRevLett.104.253602>
- 251 [8]. Riek C et al., Subcycle quantum electrodynamics, *Nature* 541, 376–379 (2017). <https://doi.org/10.1038/nature21024>
- 252 [9]. Lin Q, Zheng J, Becker W, Subcycle pulsed focused vector beams, *Phys. Rev. Lett.* 97, 253902 (2006).
253 <https://doi.org/10.1103/PhysRevLett.97.253902>
- 254 [10]. Kizmann M et al., Subcycle squeezing of light from a time flow perspective, *Nat. Phys.* 15, 960–966 (2019).
255 <https://doi.org/10.1038/s41567-019-0560-2>
- 256 [11]. Guedes TLM et al., Spectra of ultrabroadband squeezed pulses and the finite-time unruh-davies effect, *Phys. Rev.*
257 *Lett.* 122, 053604 (2019). <https://doi.org/10.1103/PhysRevLett.122.053604>
- 258 [12]. Günter G et al., Sub-cycle switch-on of ultrastrong light–matter interaction, *Nature.* 458, 178–181 (2009).
259 <https://doi.org/10.1038/nature07838>
- 260 [13]. Schubert O et al., Sub-cycle control of terahertz high-harmonic generation by dynamical bloch oscillations,
261 *Nat. Photonics.* 8, 119–123 (2014). <https://doi.org/10.1038/nphoton.2013.349>
- 262 [14]. Carlson DR et al., Ultrafast electro-optic light with subcycle control, *Science.* 361, 1358–1363 (2018).
263 <https://doi.org/10.1126/science.aat6451>
- 264 [15]. Shih Y, Entangled biphoton source - property and preparation, *Reports on Prog. Phys.* 66, 1009–1044 (2003).
265 <https://doi.org/10.1088/0034-4885/66/6/203>
- 266 [16]. Iskhakov TS et al., Polarization-entangled light pulses of 105 photons, *Phys. Rev. Lett.* 109, 150502 (2012).
267 <https://doi.org/10.1103/PhysRevLett.109.150502>
- 268 [17]. Svozilik J, Peřina J, J. P. Torres JP, High spatial entanglement via chirped quasi-phase-matched optical parametric
269 down-conversion, *Phys. Rev. A* 86, 052318 (2012). <https://doi.org/10.1103/PhysRevA.86.052318>
- 270 [18]. Brida G et al, Detection of multimode spatial correlation in pdc and application to the absolute calibration of a ccd
271 camera, *Opt. Express.* 18, 20572–20584 (2010). <https://doi.org/10.1364/OE.18.020572>
- 272 [19]. Agafonov IN, Chekhova MV, G. Leuchs G, Two-color bright squeezed vacuum, *Phys. Rev. A* 82, 011801 (2010).
273 <https://doi.org/10.1103/PhysRevA.82.011801>
- 274 [20]. Kitaeva GK et al., Generation of optical signal and terahertz idler photons by spontaneous parametric down-
275 conversion, *Phys. Rev. A* 98, 063844 (2018). <https://doi.org/10.1103/PhysRevA.98.063844>
- 276 [21]. Haase B et al., Spontaneous parametric down-conversion of photons at 660 nm to the terahertz and sub-terahertz
277 frequency range, *Opt. Express.* 27, 7458–7468 (2019). <https://doi.org/10.1364/OE.27.007458>
- 278 [22]. Kuznetsov KA et al., Nonlinear interference in the strongly nondegenerate regime and schmidt mode analysis, *Phys.*
279 *Rev. A* 101, 053843 (2020). <https://doi.org/10.1103/PhysRevA.101.053843>
- 280 [23]. Arnaut HH, Barbosa GA, Orbital and intrinsic angular momentum of single photons and entangled pairs of photons
281 generated by parametric down-conversion, *Phys. Rev. Lett.* 85, 286–289 (2000).
282 <https://doi.org/10.1103/PhysRevLett.85.286>
- 283 [24]. Law CK, Eberly JH, Analysis and interpretation of high transverse entanglement in optical parametric down
284 conversion, *Phys. Rev. Lett.* 92, 127903 (2004). <https://doi.org/10.1103/PhysRevLett.92.127903>
- 285 [25]. Straupe SS et al., Angular schmidt modes in spontaneous parametric down-conversion, *Phys. Rev. A* 83, 060302
286 (2011). <https://doi.org/10.1103/PhysRevA.83.060302>
- 287 [26]. Dayan B, Theory of two-photon interactions with broadband down-converted light and entangled photons, *Phys. Rev.*
288 *A* 76, 043813 (2007). <https://doi.org/10.1103/PhysRevA.76.043813>
- 289 [27]. Jovanovic I, Ebberts CA, Barty CPJ, Hybrid chirped-pulse amplification, *Opt. Lett.* 27, 1622–1624 (2002).
290 <https://doi.org/10.1364/OL.27.001622>

- 291 [28]. Harris SE, Chirp and compress: toward single-cycle biphoton, Phys. Rev. Lett. 98, 063602 (2007).
292 <https://doi.org/10.1103/PhysRevLett.98.063602>
- 293 [29]. Horoshko DB, Kolobov MI, Generation of monocycle squeezed light in chirped quasi-phase-matched nonlinear
294 crystals, Phys. Rev. A 95, 033837 (2017). <https://doi.org/10.1103/PhysRevA.95.033837>
- 295 [30]. Horoshko DB, Kolobov MI, Towards single-cycle squeezing in chirped quasi-phase-matched optical parametric
296 down-conversion, Phys. Rev. A 88, 033806 (2013). <https://doi.org/10.1103/PhysRevA.88.033806>
- 297 [31]. Law CK, Walmsley IA, Eberly JH, Continuous frequency entanglement: Effective finite hilbert space and entropy
298 control, Phys. Rev. Lett. 84, 5304–5307 (2000). <https://doi.org/10.1103/PhysRevLett.84.5304>
- 299 [32]. Horoshko DB et al., Bloch-messiah reduction for twin beams of light, Phys. Rev. A 100, 013837 (2019).
300 <https://doi.org/10.1103/PhysRevA.100.013837>
- 301 [33]. Fedorov M, Miklin N, Schmidt modes and entanglement, Contemp. Phys. 55, 94–109 (2014).
302 <https://doi.org/10.1080/00107514.2013.878554>
- 303 [34]. Grice WP, U'Ren AB, Walmsley IA, Eliminating frequency and space-time correlations in multiphoton states, Phys.
304 Rev. A 64 (2001). <https://doi.org/10.1103/PhysRevA.64.063815>